Mechanical performances of cement-gypsum composite material containing a weak interlayer with different angles

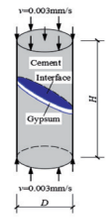

Prestaciones mecánicas de un material compuesto por cemento con una capa intermedia débil de yeso a diferentes ángulos

Pingping Luo[1], Shuren Wang[1,2*], Paul Hagan[2], Qingxiang Huang[3], Chen Cao[4], Kanchana Gamage[2]

[1] International Joint Research Laboratory of Henan Province for Underground Space Development and Disaster Prevention, Henan Polytechnic University, Jiaozuo 454003, China
[2] School of Minerals and Energy Resources Engineering, University of New South Wales, Sydney, NSW 2052, Australia
[3] College of Engery Engineering, Xi'an University of Science and Technology, Xi'an 710054, China
[4] School of Civil, Mining and Environmental Engineering, University of Wollongong, Wollongong, NSW 2522, Australia
[*] Corresponding author, e-mail: w_sr88@163.com

DOI: http://dx.doi.org/10.6036/9191 | Recibido: 01/04/2019 • Inicio Evaluación: 01/04/2019 • Aceptado: 03/05/2019

RESUMEN

- La estabilidad de la masa rocosa en ingeniería depende principalmente de las propiedades mecánicas del plano estructural. Es difícil estudiar las propiedades mecánicas del macizo rocoso sin tener en cuenta la ocultación del plano estructural. Para estudiar la influencia de la capa intermedia débil en el comportamiento mecánico de materiales similares a rocas con diferentes ángulos, espesores y parámetros mecánicos, se realizaron los ensayos de compresión en materiales de cemento con capa intermedia débil de yeso, combinados con el análisis de criterios de Mohr-Coulomb y la prueba de modelado FLAC3D. Los resultados muestran que la presión de confinamiento y la capa intermedia débil juegan el papel de control en los modos de resistencia, deformación y falla del material similar a la roca. La presión de confinamiento puede restringir eficazmente la rigidez y el debilitamiento de la fuerza debido a la débil capa intermedia del material similar a una roca. La resistencia, el módulo elástico y las características de falla del material similar a una roca muestran fuertes efectos estructurales. El ángulo de inclinación del plano estructural es cercano a los 60°, el debilitamiento de la resistencia y la rigidez es más evidente. Cuando el ángulo de inclinación del plano estructural es cercano a 0° y 90°, el material compuesto se caracteriza principalmente por fallas de división; cuando el ángulo de inclinación es cercano a 15°, el material presenta principalmente fallas de cizallamiento. En otros casos, el material presenta principalmente modos de fallo por tracción y cizallamiento. Los resultados pueden proporcionar la base teórica y técnica para una práctica de ingeniería similar.
- **Palabras clave:** Material rocoso, Capa intermedia débil, Ensayo de compresión, Simulación numérica.

ABSTRACT

The stability of engineering rock mass mainly depends on the mechanical properties of the structural plane. It is difficult to study the mechanical properties of the rock mass without considering the concealment of the structural plane. To study the influence of weak interlayer on mechanical performances of rock-like material with different angles, thicknesses and mechanical parameters, the compression tests were carried out on cement material with gypsum weak interlayer, combined with Mohr-Coulomb criterion analysis and FLAC3D modelling test. Results show that the confining pressure and the weak interlayer play the control role on the strength, deformation and failure modes of the rock-like material. The confining pressure can effectively restrain the stiffness and strength weakening due to weak interlayer of the rock-like material. The strength, elastic modulus and failure characteristics of the rock-like material show strong structural effects. The inclination angle of the structural plane is close to 60°, the strength and stiffness weakening are more obvious. When the inclination angle of the structural plane is close to 0° and 90°, the composite material is mainly characterized by splitting failure; when the inclination angle is close to 15°, the material mainly exhibits shear failure. In other cases, the material mainly exhibits tensile and shear failure modes. The results can provide the theoretical and technical basis for similar engineering practice.

Keywords: Rock-like material, Weak interlayer, Compression test, Numerical simulation.

1. INTRODUCTION

Rock masses within the engineering scale are usually cut into discontinuities by one or several sets of structural planes such as faults, joints, weak interlayers, etc., which enhance the anisotropy of the rock mass in mechanical properties and exhibit complex mechanical characteristics. The stability of rock mass and its deformation and failure depend mainly on the nature of various structural planes and the cutting degree of the rock mass. Engineering practice shows that the failure of rock mass in the slope slide, the foundation slippage, and the collapse of surrounding rock of the tunnel occur mostly along the weak structural plane [1-2]. The structure plane usually plays a leading role in the deformation and failure of the rock mass.

It is always a hot topic to research on the mechanical properties of structural planes over the past years [3-5]. For the mechanical properties of the structural plane, theoretical analysis usually assumes that rock mass is a superposition of the rock and the structural plane. Based on classical strength criterion, such as Mohr-Coulomb criterion, the calculation result is often different from the actual rock mass. The test methods can reflect the properties of small-scale rock mass, but can not reflect the behaviors of the large-scale engineering [6]. While the numerical method

can strictly follow the mechanics rules and establish complex engineering models, which is widely used in geotechnical engineering based on the indoor and outdoor tests [7].

Since the stability of rock mass in the slope engineering, foundation engineering, and underground engineering mainly depends on the mechanical properties of the structural planes, while the structural planes are often hidden in the rock mass, and the related research has not been clear, so it is very important to study the strength and deformation characteristics of rock mass to ensure the safety of the engineering practice by using rock-like material with different structural planes.

2. STATE OF THE ART

Theoretical analysis, laboratory and field test and numerical simulation are usually used to investigate the mechanical properties of rock mass with structural planes. For the field test, Xu and Yan performed a series of large-scale direct shear tests to evaluate the mechanical properties of a weak intercalated layer in the rock mass of a slope, and they derived the constitutive function for normal deformation from the test results [8]. Due to the intermediate principal stress does indeed have an influence on rock strength, Al-Ajmi and Zimmerman established Mogi-Coulomb failure criterion by considering the parameters' relationship between Coulomb criterion and Mogi criterion [9]. Moreover, based on the total differential rule of multivariate functions, other researchers also established the strength criterion of jointed rock mass taking into the effect of joint dip angle. Although the field test data is of some representative, it is difficult to obtain widespread application due to the time-consuming, costly and inefficient of the field test.

Since natural rock mass has heterogeneity, anisotropy, and complicated structural characteristics, many researchers studied mechanical properties of rock mass by carrying out indoor experiments with similar materials. For examples, using the advanced three-dimensional reconstruction technology, Tien et al. analyzed the failure process and characteristics of layered similar materials, they summarized the failure modes under different inclination angles and confining pressures, and proposed Tien-Kuo failure criterion [10-11]. Based on equivalent deformation assumption, Zhang analyzed microscopic deformation of fractured rock mass and theorized the expression of the deformation parameters [12]. Xu et al. adopted a self-made device to test the mechanical properties of weak interlayer in rock mass [13-15]. Kumar and Verma investigated an anisotropic shear behavior of joint replicas under constant normal loading and they proposed an anisotropic peak shear strength model [16]. For the single continuous jointed rock mass with different dip angles, Wang et al. established a damage constitutive model by considering the coupling of structural effect and loading conditions [17-18]. To understand the influence of the combination characteristics of the two intersected structural planes on mechanics parameters, Yang et al. investigated the effect of fracture morphology on mechanical properties and failure modes of samples [19-20]. The above experiments focused on the static load test without considering the loading rate effect.

Field tests tend to be costly and time-consuming and laboratory tests cannot fully reproduce the properties of macro engineering rock mass, most researchers often adopt numerical simulations that strictly follows the mechanical rules to establish complex geotechnical engineering models. By using FLAC^{3D} to construct a stratified rock mass model, Zhou et al. found that the compressive strength of rock sample initially decreased and then increased with inclination of structure plane increasing [21]. Through numerical simulation of uniaxial and triaxial compression, Zuo et al. found that the inclination angle and the confining pressure substantially influenced the mechanical behaviors of layered rock mass [22]. Xu et al. found that the influence of weak interlayer on fracture of rock mass was mainly determined by the number, thickness and spacing of interlayers by combining numerical simulation with fracture theory of rock mechanics [23-24]. By synthesizing a rock mass model that couple discrete fracture networks with a discrete element grain-based model, Farahmandet al. characterized the mechanical properties of moderately jointed rock mass under confined and unconfined conditions and investigated the scale dependency of the rock mass properties using the concept of representative element volume [25]. However, numerical simulations of weak interlayers focus on the number and spacing of weak interlayer. It remains unclear how the physical and mechanical parameters of weak interlayers and their interactions affect the strength and deformation of rock mass. Moreover, it is important to combine laboratory and/or field tests to improve the accuracy of numerical simulation while studying the deformation and failure characteristics of real rock mass.

In this study, combined laboratory compression tests with FLAC^{3D} numerical simulation, the strength, deformation, and failure characteristics of rock-like materials under different loading conditions were investigated, and the inclination angles of weak structural planes along with physical and mechanical parameters were studied. The remainder of this study is organized as follows. In Section 3, the rock-like materials (cement and plaster) are prepared and the research methods are introduced. In Section 4, the mechanical performances of the rock-like materials with different weak planes are analyzed and discussed. Section 5 summarizes the conclusions.

3. METHODOLOGY

3.1. SPECIMEN PREPARATION

As shown in Fig. 1, there were nine types of specimens included cement sample, gypsum sample, and seven groups of rock-like

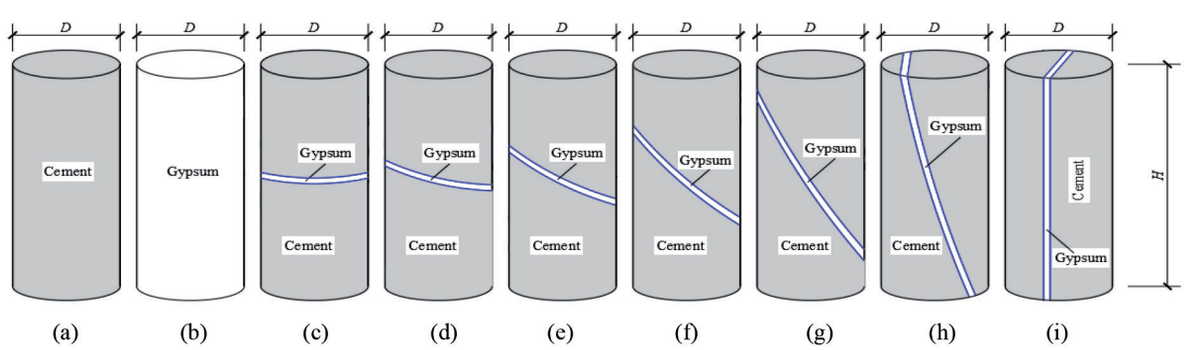

Fig. 1 Rock-like material specimens.(a)Cement, (b)Gypsum, (c)β=0°, (d)ç=15°, (e)β=30°, (f)β=45°, (g)β=60°, (h)β=75°, (i)β=90°

Material	β (°)	Bulk modulus (MPa)	Shear modulus (MPa)	Density (kg/m³)	Cohesion (MPa)	Friction angle (°)	Tensile strength (MPa)	Expansion angle (°)
Cement	0	424	318	2500	7.68	45	5.33	10
	15	314	236					
	30	287	215					
	45	131	98					
	60	83	62					
	75	176	132					
	90	367	275					
Gypsum	0	184	85	1900	1.24	30	1.16	5
	15	136	63					
	30	124	57					
	45	57	26					
	60	36	17					
	75	76	35					
	90	159	73					

Table I. The calculation parameters of cement and gypsum materials

Shear stiffness (GPa/m)	Normal stiffness (GPa/m)	Cohesion (MPa)	Friction angle (°)	Tensile strength (MPa)
100	100	0.002	0	0

Table II. Mechanical parameters of interface

materials with weak interlayer. The average diameter *D* of the cylindrical sample was 41.6 mm, and the average height *H* of the cement sample, gypsum sample, and the composite cylindrical sample was 98.0 mm, 98.0 mm, and 96.3 mm, respectively. A modified Portland cement grout was used to cast samples and the cement named Stratabinder HS was produced by the Minova Company, Australia. The Hydrostone TB gypsum (>95 % $CaSO_4 \cdot 1/2H_2O$, <5 % Portland cement, Australia) was used to cast weak interlayer. The water/cement ratio of cement sample was 0.35 and that of gypsum sample was 0.42 [26]. The weak interlayer of each rock-like material was at an average thickness of 2.5 mm and different dip angles, such as 0°, 15°, 30°, 45°, 60°, 70°, and 90°, respectively. The binder was mixed Epoxy 14210 resin with the adhesive tensile of 1.9 kPa (A rapid-curing, general purpose adhesive/encapsulant was from Danvers, North America, Fig. 2, See section: supplementary material).

3.2. COMPRESSIVE TEST

The compression tests of the specimens were conducted by using MTS815 electro-hydraulic servo-controlled rock mechanics testing system.

Six groups of samples have been tested (each group at least three specimens under each condition):

Group 1 (cement samples, the loading rate was 0.003 mm/s for each sample) was conducted the compressive strength experiment under different confining stresses of 0.0, 2.0, 4.0 and 6.0 MPa, respectively.

Group 2 (gypsum samples, the loading rate was 0.003 mm/s for each sample) was conducted the compressive strength experiment under different confining stresses of 0.0, 1.0, 2.0, and 3.0 MPa, respectively.

Group 3 (cement samples) and Group 4 (gypsum samples) were conducted the unconfined compressive strength (UCS) experiments under different loading rates of 0.003, 0.3, and 3.0 mm/s.

Group 5 (rock-like materials with weak interlayer at seven dip angles, the loading rate was 0.003 mm/s for each sample) was conducted the compressive strength experiment under different confining stresses of 0.0, 1.5 and 3.0 MPa, respectively.

Group 6 (rock-like materials with weak interlayer at seven dip angles) was conducted the unconfined compressive strength experiment under different loading rates of 0.003, 0.3, and 3.0 mm/s, respectively.

There were at least 3 samples under static loading and 5 samples under dynamic loading condition for each group, respectively. The measure of axial load and axial displacement values could be performed in real time by data acquisition system automatically.

3.3. NUMERICAL SIMULATION

According to the rock-like material specimens, the computation models were established by using FLAC^{3D}. The calculation parameters of cement and gypsum materials were listed in Table I. The mechanical parameters of the weak interlayer regarded as an interface element in the model were listed in Table II. Mohr-Coulomb criteria was used in the numerical calculation. As seen from

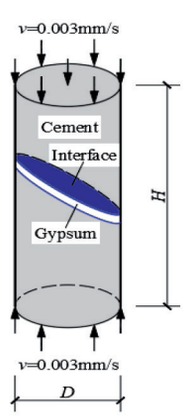

Fig. 3 Loading mode

Fig. 3, the speed acting on both ends of the model was adopted as the loading mode, which was 3×10^{-6} m/s.

The numerical method was as follows: firstly, the test curve was fitted to verify the rationality of the calculation parameters. Then, the failure modes of the weak interlayer with different dip angles were analyzed, and the sensitivity analysis of the influence of parameters of the weak layer on the compressive strength of the specimen was analyzed.

4. RESULT ANALYSIS AND DISCUSSION

4.1. EXPERIMENTAL RESULTS

4.1.1. Dip angle effect of weak interlayer on elastic modulus

Fig. 4 (See section: supplementary material) showed the relationship between the elastic modulus *E* of rock-like specimens and the dip angle of the weak interlayer β.

As seen from Fig. 4 (See section: supplementary material), under the same confining pressure, the elastic modulus *E* decreased first and then increased with increasing of β. The *E* values were almost identical (9 GPa) when β= 0° and β= 90°. When β= 60°, the *E* value was minimal and the deformation resistance was the worst, which indicated that the specimen showed the weakest stiffness. With increasing of confining pressure, the elastic modulus *E* showed higher gradually.

When β= 45° and β= 60°, the *E* values at the confining pressure of 1.5 MPa increased 30% and 60% than that in none confining pressure conditions, respectively. Similarly, the *E* values at the confining pressure of 3.0 MPa increased 17% and 36% than that at the confining pressure of 1.5 MPa, respectively.

Therefore, the confining pressure could effectively restrain the stiffness weakening of rock-like specimens, especially when the dip angle of weak interlayer was 45° ≤ β≤60°.

4.1.2. Confining pressure effect on compressive strength

Fig. 5 showed the strength curves of all specimens under different confining pressures. As seen from Fig. 6(a), with increasing of the confining pressure, the compressive strength of each specimen increased greatly. As seen from Fig. 6(b), for rock-like specimen with weak interlayer, the compressive strength of the specimen decreased when β changed from 0° to 60°, then increased when β changed from 60° to 90°, gradually. The compressive strength is minimal when β = 60°, so, the weak interlayer exerted dominant control of the deterioration of mechanical properties of rock-like materials when β approached about 60°.

Fig. 5 also indicated some interesting results that differed from previous theoretic predictions according to the Mohr-Coulomb failure criterion. Fig. 6 shows that the strength of rock mass lies between the strength of the structural plane and that of the intact rock. Specifically, the strength of rock-like materials largely depends on rock strength when $\beta<\beta_1$ or $\beta>\beta_2$, whereas it is deter-

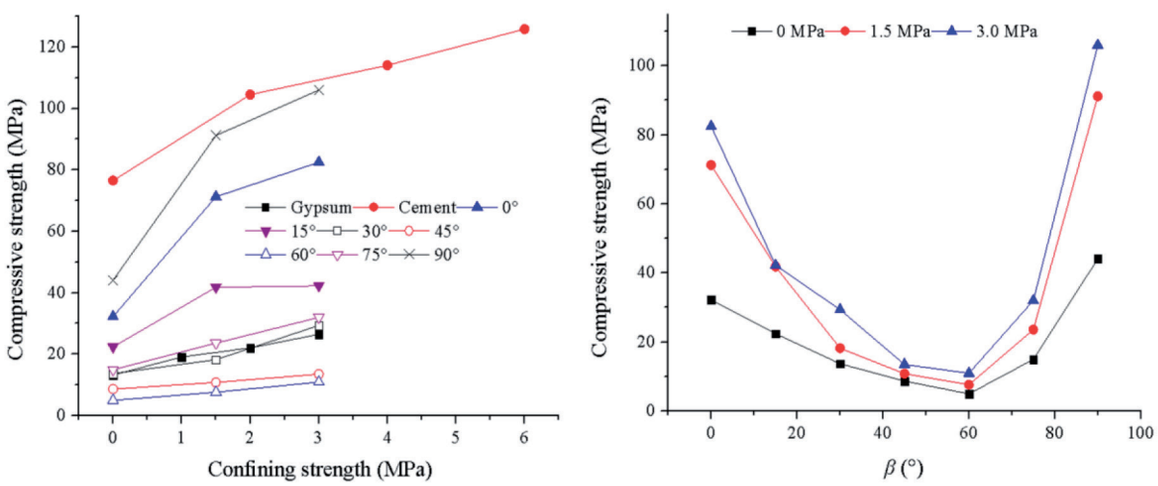

Fig. 5 Compressive strength curves of specimens. (a) Relationship between compressive strength and confining pressure, (b) Relationship between compressive strength and β

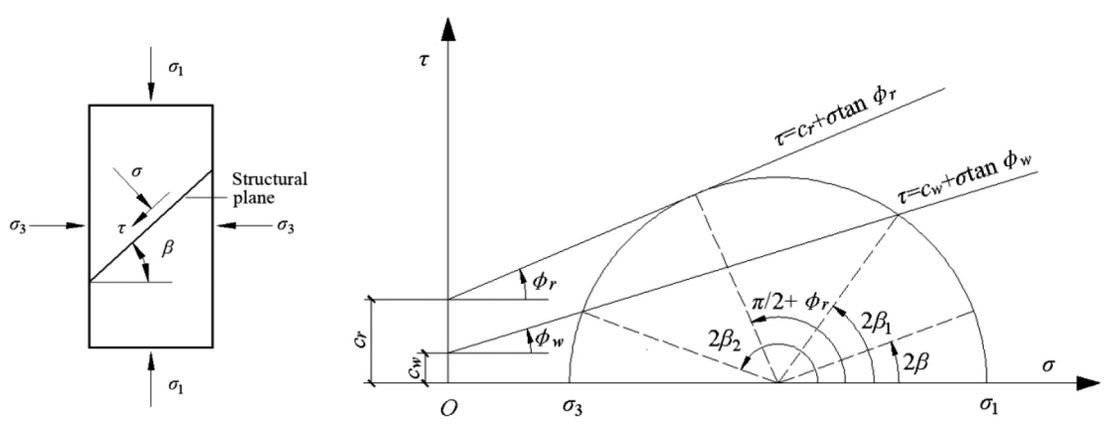

Fig. 6 Mechanical characteristics of rock mass with structural plane. (a) Stress mode of specimen, (b) Mohr-Coulomb failure criterion of rock mass

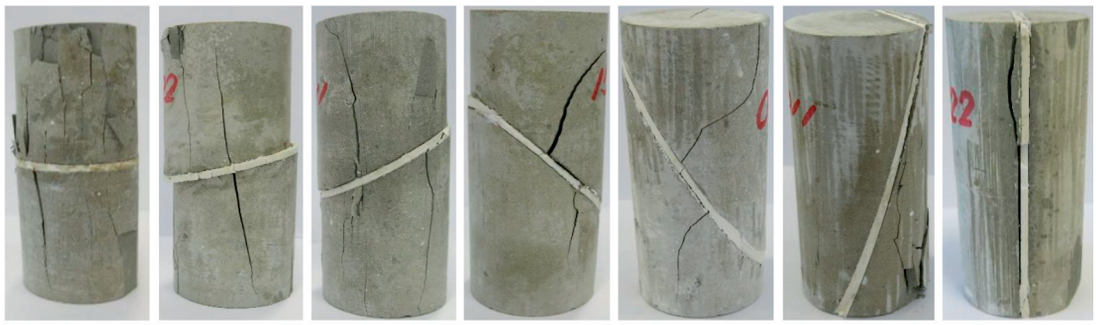

Fig. 8 Failure modes of specimens under uniaxial compression. (a)β=0°, (b)β=15°, (c)β=30°, (d)β=45°, (e)β=60°, (f)β=75°, (g)β=90°

mined by the strength of structural plane when $\beta_1 \leq \beta \leq \beta_2$. As seen from Fig. 5, the compressive strength of rock-like materials with β between 45° and 60° was lower than that of gypsum specimen under the same confining pressure. Moreover, the compressive strength of rock-like materials with β = 0° and β = 90° was also lower than that of cement specimen.

The discrepancy between the experimental results and theoretical prediction could be derived from the fact that the Mohr-Coulomb failure criterion only considered the shear failure caused by shear strength and ignored splitting failure caused by tensile strength of rock mass. Moreover, the weak interlayer, especially that with a certain thickness, complicated the mechanical properties of rock mass and could not be regarded as a simple weak structural plane. In fact, Tien et al. also found that the theoretical compressive strength differed from that of the laboratory test when $\beta \leq \varphi_w$ or = 90° [27].

σ_1-the maximum principal stress,σ_3-the minimum principal stress, c_r-cohesion of rock, c_w-cohesion of structural plane, φ_r-friction angle of rock, φ_w-friction angle of structural plane, β-angle between the structural plane and plane of the maximum principal stress.

4.1.3. Loading rate effect on UCS

Fig. 7 (See section: supplementary material) showed the UCS curves of different specimens under the loading rates of 0.003, 0.3, and 3 mm/s. The biomodal inverted bell curves indicated that the UCS reached the minimum values when β = 60° under different loading rates (Fig. 7a, See section: supplementary material). Moreover, with increasing of the loading rate, the UCS increased gradually. Interestingly, the UCS of the specimens were lower than that of the gypsum specimen (Plaster) when 30° ≤ β≤75°.

4.1.4. Failure modes of rock-like specimens with weak interlayer

As shown in Fig. 8, when β = 0°, the cracks on the specimen were nearly parallel to the axis direction of the loading and there was no obvious shear fracture, indicating that the main failure mode was the splitting failure related to tension. When β = 15°, the upper part of the specimen slipped along the weak interlayer, the main crack was normal to the weak interlayer and penetrated that from the upper to the lower part of the specimen, which showed the shear-tension failure mode. When β = 30°, there was shear slip cracks along the interface with two splitting cracks almost parallel to the loading direction on the surface of the specimen, which indicated an overall tension-shear failure mode. When β = 45° and β = 60°, the staggered two cracks were normal to the weak interlayer and shear cracks occur along the interface, which indicated the tension-shear failure mode also. In the case of β = 75° and β = 90°, the tension cracks mainly slipped along the interface of the specimens, which indicated the splitting failure related to tension.

When 30°≤ β ≤ 60°, except shear failure, there showed the obvious tension cracks in the samples, the composite failure caused the lower compressive strength values, especially when β = 60°. Which was consistent with the results in Figs. 5(b), 6, and 7(a).

4.1.5. Confining pressure effect on post-peak characteristics of σ-ε curve

Fig. 9 showed the stress-strain curves of specimens with weak interlayer at different dip angles. As seen from Fig. 9, Under the same confining pressure, the shape of the compression curve with different dip angles of the weak interlayer was different, which showed that the slope, peak strength and post-peak characteristics of the curve were different. As analyzed in Figs. 4 and 5, the slope and peak strength of the curve were the smallest when β = 60°. For specimens with the same inclination angle of the weak interlayer, with the confining pressure increasing, the slope and peak strength increased, and that slowed down the decline after the peak, but showed better ductility of the specimen. In addition, in the initial elastic stage, the smaller the confining pressure, the longer the closure time of the original fracture, the more obvious the concave phenomenon of the curve.

The value of β affected the brittleness-ductility transition and the critical confining pressure. For example, under the confining pressure of 3.0 MPa, the specimen showed brittleness-ductility transition when 0°≤β≤60°. However, the specimen still showed brittleness when β = 75° or β = 90°. With the confining pressure increasing, the strain hardening occurred in specimens when 30°≤ β ≤ 60°. This effect was obvious for specimens when β = 45° or 60° [28].

It could be seen that the confining pressure, as an external factor, played an auxiliary role in the stability of the structural plane, especially in strengthening the weakened zone of the structural plane with an inclination of 45° and 60°. The peak strength of the specimens with β = 0° or β = 90° was lower than that of the cement specimens, to some extent, the peak strength of the specimens was always lower than that of the rock specimens as long as there was a soft interlayer in the specimen, regardless of its dip angle. Generally, with the confining pressure increasing, the pre-peak deformation of specimens increased. But for the specimen with β = 60°, when the confining pressure was 0 MPa, the pre-peak deformation was the largest, while the confining pressure were 1.5 MPa and 3.0 MPa, the pre-peak deformations were basically the same.

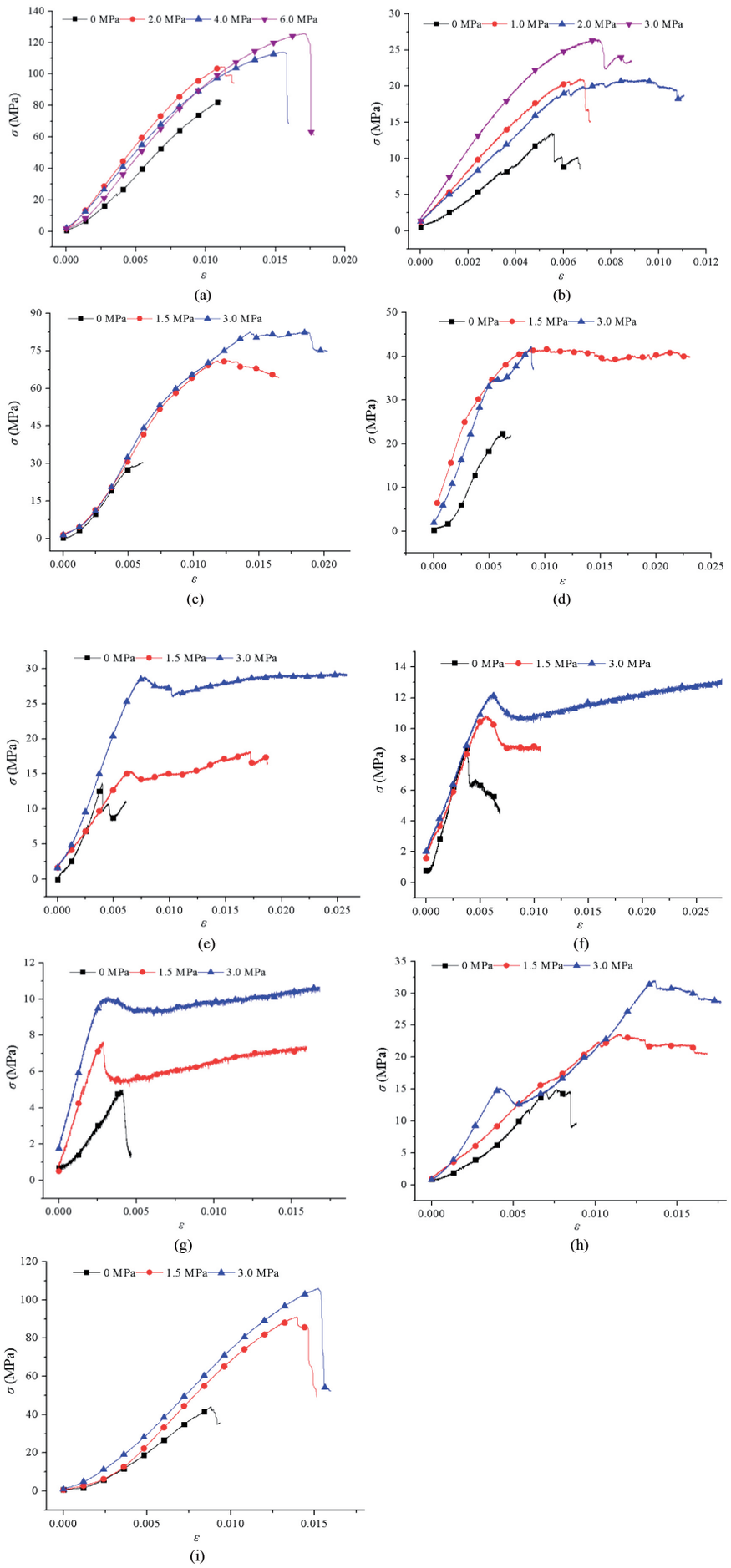

Fig. 9 Curves of axial stress vs axial strain. (a)Cement, (b)Gypsum, (c)β=0°, (d)β=15°, (e)β=30°, (f)β=45°, (g) β=60°, (h)β=75°, (i)β=90°

4.2. NUMERICAL TEST RESULTS

4.2.1. Elastic modulus and tensile strength effects of weak interlayer on UCS

As shown in Fig. 10 (See section: supplementary material), for the uniaxial compressive strength values of the rock-like materials, the numerical simulation results fitted well to the laboratory tests, which showed that the computational parameters were reasonable in the numerical simulation. Then a series of numerical tests were conducted on the sensitive analysis of the parameters of the weak interlayer.

As seen from Fig. 11(a) (See section: supplementary material), with increasing of the elastic modulus of the weak interlayer, the UCS of rock-like specimens increased gradually when β<60°. However, for a given β in Fig. 11(b) (See section: supplementary material), the tensile strength of the weak interlayer had nearly no effect on the UCS of specimens.

4.2.2. Shearing parameter effect of weak interlayer on UCS

As shown in Fig. 12 (See section: supplementary material), with increasing of the cohesion and friction angle, the two key shearing parameters of the weak interlayer, the UCS of rock-like specimens linearly increased when β≤15°. When β= 0° and 15°, comparison the cohesion of the weak interlayer 2.5 MPa and 0 MPa, he UCS values of rock-like materials increased 25.3% and 25.1%, respectively. Other cases were small increments. The effect of the tensile strength of the weak layer on UCS was also the same. It can be seen that the influence of the shearing parameters of the weak layer on UCS were related to β. When the β was smaller, the influence was the greater.

4.2.3. Parameters synchronous effects of weak interlayer on UCS

In the actual reinforcement project, such as grouting and bolt support, it is impossible to affect only the single mechanical parameters of the weak interlayer. To evaluate the synchronous variation of the mechanical parameters of the weak layer influencing on UCS of the specimens, the special parameter *n* was defined as follows:

$$n = \frac{K}{K_0} = \frac{G}{G_0} = \frac{C}{C_0} = \frac{\tan\phi}{\tan\phi_0} = \frac{\sigma_t}{\sigma_{t0}} \quad (1)$$

where K and K_0 were the respective bulk modulus of weak interlayer and cement, G and G_0 were the respective shear modulus of weak interlayer and cement, C and C_0 were the respective cohesion of weak interlayer and cement, Φ and Φ_0 were the respective friction

angle of weak interlayer and cement, and σ_t and σ_{t0} were respective tensile strength of weak interlayer and cement. These values of K_0, G_0, C_0, Φ_0, and σ_{t0} were listed in Table I.

As shown in Fig. 13 (See section: supplementary material), when $n \leq 0.8$, $\beta = 0°$ and 15°, with increasing of n, the UCS values increased obviously firstly, and then increased slowly linearly. When $\beta = 30°$, 45°, 60°, and 75°, the parameter n has minimal effect on UCS (4% UCS increase between $n = 2$ and $n = 1$, when $\beta = 75°$, and less than 0.5% UCS in other cases). When $\beta = 90°$, the UCS values increased linearly with the increase of n, resulting a largest increase of 13% UCS comparing the cases of $n = 2$ and $n = 1$.

4.2.4. Thickness effect of weak interlayer on UCS

As seen from Fig. 14 (See section: supplementary material), when the weak interlayer was the thicker, the UCS values were lower. But the decrease was related to β. When β=75°, the UCS values were reduced by 35% and the decrease was the largest, followed by 27% when β=15°, 26% when β=0°, and 12% when β=90°. The smallest decrease was less than 1.5% when β=45°. But for β=60°, the thicker the weak layer was, the more the UCS values increased. When the thickness of the weak layer was 5 mm, the UCS values increased about 6% compared to the thickness of 1 mm.

4.2.5. Mechanical parameter effect of interface on UCS

In FLAC^{3D}, the shear and normal stiffness values of the interface element was set ten times the equivalent stiffness of the neighboring zones using Eq. (2).

$$k_s = k_n = 10\left[\frac{K + \frac{4}{3}G}{\Delta z_{\min}}\right] \tag{2}$$

where K and G are the bulk and shear modulus of the neighboring zone, respectively, and $\Delta z_{\min}$ is the smallest width of the adjacent zone in the normal direction.

To reveal the relationship between the interface stiffness and the rock-like materials, we introduced Eq. (2). As seen from Fig. 15 (See section: supplementary material), when $\beta = 0°$, 15°, and 90°, the higher interface stiffness was associated with the stronger rock mass. However, the effects of interface stiffness were very small when $30° \leq \beta \leq 75°$ (Fig. 15(a), See section: supplementary material). The tensile strength of the interface had no effect on UCS of rock-like materials at all β values (Fig. 15(b), See section: supplementary material). The cohesion of interface greatly increased the UCS only when the cohesion was greater than 200 kPa and $\beta < 90°$ (Fig. 15(c), See section: supplementary material). The internal friction angle of interface had a great influence on UCS when β was small than 60°. When β was smaller, the more effect on UCS by the internal friction angle (Fig. 15(d), See section: supplementary material).

4.2.6. Failure simulation of rock-like material with weak interlayer

As seen from Fig. 16 (See section: supplementary material), when $\beta = 0°$, the shear and tensile failure occurred in the weak interlayer and tensile failure occurred in the cement. When $\beta = 15°$, the shear failure occurred mainly in the weak interlayer and cement. When $30° \leq \beta \leq 60°$, the tensile-shear failure zone appeared in the cement. When $\beta = 75°$, the shear failure zone appeared in the weak interlayer and its lower left part, while tensile failure zone appeared in the lower right part of the weak interlayer. When $\beta = 90°$, the shear failure zone occurred in the weak interlayer and the tensile failure zone occurred in the outer edge of the cement orthogonal to the weak interlayer. The results were highly consistent with those obtained from laboratory compression tests (Fig. 8), also demonstrating the validity of the simulation approach.

CONCLUSIONS

To study the influence of weak interlayer's dip angles, thickness, mechanical parameters, and loading conditions on the strength, deformation, and failure characteristics of rock-like materials, the laboratory compression tests, numerical simulation, and theoretical analysis were conducted. The main conclusions are as follows:

(1) Confining pressure can effectively restrain the weakening effect of structural plane on the stiffness and strength of rock mass. When weak interlayer's dip angle $\beta = 45°$ and $\beta = 60°$, the elastic modulus values at the confining pressure of 1.5 MPa increased 30% and 60% than that in none confining pressure conditions, respectively. Similarly, the elastic modulus E values at the confining pressure of 3.0 MPa increased 17% and 36% than that at the confining pressure of 1.5 MPa, respectively. Therefore, the confining pressure could effectively restrain the stiffness weakening of rock-like specimens, especially when the dip angle of weak interlayer was $45° \leq \beta \leq 60°$.

(2) The elastic modulus, compressive strength and failure characteristics of the rock mass show obvious structural effects. With the increase of the dip angle of the structural plane, the elastic modulus and compressive strength of the rock mass first decrease and then increase. When the weak structural plane is thicker, the compressive strength of the rock mass is smaller. When the inclination angle of the structural plane is close to 60°, the elastic modulus and the compressive strength are the smallest, but at this time, the weak structural plane become thicker, the compressive strength slightly increases.

(3) The mechanical parameters of interlayer or interface also influence the compressive strength of rock mass in a manner that depends on the dip angle of the interlayer. The stiffness and shear parameters of the interface are positively correlated with rock strength only when the dip angle is smaller than 45°. When the inclination angle of the structural plane is close to 0° and 90°, the composite material is mainly characterized by splitting failure; when the inclination angle is close to 15°, the material mainly exhibits shear failure. In other cases, the material mainly exhibits tensile and shear failure modes.

In engineering practice, the composition and structure of weak structural plane of rock mass are complex. Rock mass generally contains multiple layers and even cross weak structural planes and reside in diverse surroundings of various temperature and pressure. This study mainly analyzed the mechanical properties of rock mass with a single weak interlayer. Future studies on rock mass with multiple weak structural planes and under high pressure conditions will provide additional insights to further improve rock mass engineering practices.

REFERENCES

[1] Wang SR, Xu DF, Hagan P, Li CL. "Fracture characteristics analysis of double-layer rock plates with both ends fixed condition". Journal of Engineering Science and Technology Review. July 2014. Vol. 7-2. p. 60-65.
[2] Guo HR, Qiao L, Xiao YY, Ren XY. "Heat transfer enhancement of graphite-modified concrete energy piles". Journal of Power Technologies. December 2018. Vol. 98-4. p. 345-351.
[3] Feng F, Li XB, Rostami J, Li DY. "Modeling hard rock failure induced by structural planes around deep circular tunnels". Engineering Fracture Mechnics. January 2019. Vol. 205. p. 152-174. DOI: https://doi.org/10.1016/j.engfracmech.2018.10.010
[4] He ZM, Xiong ZY, Hu QG, Yang M. "Analytical and numerical solutions for shear mechanical behaviors of structural plane". Journal of Central South University. July 2014. Vol. 21-7. p. 2944-2949. DOI: https://doi.org/10.1007/s11771-014-2261-4
[5] Zhang QZ, Shen MR, Clark C. "Shearing mechanical properties of structural planes of a regular tooth rock". Materials Testing. September 2011. Vol. 53-9. p. 540-555. DOI: https://doi.org/10.3139/120.110260
[6] Duan SQ, Feng XT, Jiang Q, Liu GF, Pei SF, Fan YL. "In situ observation of failure mechanisms controlled by rock masses with weak interlayer zones in large underground cavern excavations under high geostress". Rock Mechanics and Rock Engineering, September 2017. Vol. 50-9. p. 2465-2493. DOI: https://doi.org/10.1007/s00603-017-1249-4
[7] Huang F, Zhu HH, Xu QW, Cai YC, Zhuang XY. "The effect of weak interlayer on the failure pattern of rock mass around tunnel-Scaled model tests and numerical analysis". Tunnelling and Underground Space Technology. April 2013. Vol. 35. p. 207-218. DOI: https://doi.org/10.1016/j.tust.2012.06.014
[8] Xu BT, Yan CH. "An experimental study of the mechanical behavior of a weak intercalated layer". Rock Mechanics and Rock Engineering, April 2013, Vol. 47-2. p. 791-798. DOI: https://doi.org/10.1007/s00603-013-0420-9
[9] AL-AJMI AM, Zimmerman RW. "Relation between the Mogi and the Coulomb failure criteria". International Journal of Rock Mechanics and Mining Sciences. January 2005. Vol. 42-3. p. 431-439. DOI: https://doi.org/10.1016/j.ijrmms.2004.11.004
[10] Tien YM, Kuo MC. "A failure criterion for transversely isotropic rocks". International Journal of Rock Mechanics and Mining Sciences. April 2001. Vol. 38-3. p. 399–412. DOI: https://doi.org/10.1016/S1365-1609(01)00007-7
[11] Tien YM, Kuo MC, Juang CS. "An experimental investigation of the failure mechanism of simulated transversely isotropic rocks". International Journal of Rock Mechanics and Mining Sciences. December 2006. Vol. 43-8. p. 1163-1181. DOI: https://doi.org/10.1016/j.ijrmms.2006.03.011
[12] Zhang ZQ. "Micromechanical failure characteristics and macromechanical parameter estimation of fractured rock mass with nonpenetrative fissures". Chinese Journal of Rock Mechanics and Engineering. September 2009. Vol. 28-9. p. 1945-1945.
[13] Xu BT, Yan CH, Chen HY, Zhou WS. "Experimental study of mechanical property of weak intercalated layers in slope rock mass". Rock and Soil Mechanics. November 2008, Vol. 29-11. p. 3077-3081.
[14] Liu XS, Tan YL, Ning JG, Lu YW, Gu QH. "Mechanical properties and damage constitutive model of coal in coal-rock combined body". International Journal of Rock Mechanics and Mining Sciences. October 2018. Vol. 110-10. p. 140-150. DOI: https://doi.org/10.1016/j.ijrmms.2018.07.020
[15] Du SG, Huang M, Luo ZY, Jia RD. "Similar material study of mechnical prototype test of rock structural plane". Chinese Journal of Rock Mechanics and Engineering. November 2010. Vol. 29-11. p. 2263-2270
[16] Kumar R, Verma AK. "Anisotropic shear behavior of rock joint replicas". International Journal of Rock Mechanics and Mining Sciences. December 2016. Vol. 90. p. 62-73. DOI: https://doi.org/10.1016/j.ijrmms.2016.10.005
[17] Wang J, Song WD, Fu JX. "A damage constitutive model and strength criterion of rock mass considering the dip angle of joints". Chinese Journal of Rock Mechanics and Engineering. October 2018. Vol. 37-10. p. 2253-2263. DOI: https://doi.org/10.13722/j.cnki.jrme.2018.0496
[18] Zhang SK, Wang SD, Wang LG, Sun Q. "Stability study of roadway surrounding rock under influence of local weakening of structural plane". China Safety Science Journal. July 2018. Vol. 28-7. p. 116-121. DOI: https://doi.org/10.16265/j.cnki.issn1003-3033.2018.07.019
[19] Yang H, Shan RL, Zhang JX, Wu FM, Guo ZM. "Mechanical properties of frozen rock mass with two diagonal intersected fractures". International Journal of Mining Science and Technology. July 2018. Vol. 28-4. p. 631-638. DOI: https://doi.org/10.1016/j.ijmst.2018.02.005
[20] Sun SR, Sun HY, Wang YJ, Wei JH, Liu J, Kanungo DP. "Effect of the combination characteristics of rock structural plane on the stability of a rock-mass slope". Bulletin of Engineering Geology and the Environment. March 2014. Vol. 73. p. 987-995. DOI: https://doi.org/10.1007/s10064-014-0593-9
[21] Zhou KF, Li YZ, Liu QY. "Numerical analysis of structure plane characteristic for strength of stratified rock mass". Journal of Central South University (Science and Technology). April 2012. Vol. 43-4. p. 1424-1428.
[22] Zuo SY, Ye ML, Tang XL, Xu JK. Shi WB. Numerical model and validation of failure mode for underground caverns in layered rock mass. Rock and Soil Mechanics. August 2013. Vol. 34-S1. p. 458-465.
[23] Xu K, Dai JS, Feng JW, Fu XL, Wang S, Liu C. "Application of ANSYS in discussing influence of weak interbed on rock fracture". Fault-Block Oil & Gas Field. June 2015. Vol. 22-6. p. 735-739.
[24] Li A, Shao GJ, Su JB, Liu JC, Sun Y. "Uniaxial compression test and numerical simulation for alternatively soft and hard interbedded rock mass". Journal of Hohai University (Natural Sciences). June 2018. Vol. 46-6. p. 533-538.
[25] Farahmand K, Vazaios I, Diederichs MS, Vlachopoulos N. "Investigating the scale-dependency of the geometrical and mechanical properties of a moderately jointed rock using a synthetic rock mass (SRM) approach". Computers and Geotechnics. March 2018, Vol. 95-3. p. 162-179. DOI: https://doi.org/10.1016/j.compgeo.2017.10.002
[26] Wang SR, Li DJ, Li CL, Zhang CG, Zhang YB. "Thermal radiation characteristics of stress evolution of a circular tunnel excavation under different confining pressures". Tunnelling and Underground Space Technology. April 2018. Vol. 78. p. 76-83. DOI: https://doi.org/10.1016/j.tust.2018.04.021
[27] Tien YM, Tsao PF. "Preparation and mechanical properties of artificial transversely isotropic rock". International Journal of Rock Mechanics and Mining Sciences. September 2000. Vol. 37-6. p. 1001-1012. DOI: https://doi.org/10.1016/S1365-1609(00)00024-1
[28] Cabrera-Covarrubias FG, Gómez-Soberón GM, Almaral-Sánchez JL, Arredondo-Rea SP, Gómez-Soberón MC, Corral-Higuera R. "An experimental study of mortars with recycled ceramic aggregates: deduction and prediction of the stress-strain". Materials. December 2016. Vol. 9. Article 1029. p. 1-24. DOI: https://doi.org/10.3390/ma9121029

ACKNOWLEDGEMENTS

This work was supported by the National Natural Science Foundation of China (51774112; U1810203; 51674190; 51474188), the International Cooperation Project of Henan Science and Technology Department (182102410060), the Doctoral Fund of Henan Polytechnic University (B2015-67), and Taihang Scholars Program.

SUPPLEMENTARY MATERIAL

https://www.revistadyna.com/documentos/pdfs/_adic/9191-1.pdf